MULTI-MODAL MEMS SENSING MODULE FOR EXTRATERRESTRIAL OCEANOGRAPHIC EXPLORATION

Zhijian Hao[1], Yue Zheng[1], Ethan W. Schaler[2] and Azadeh Ansari[1]*
[1]Georgia Institute of Technology, USA
[2]Jet Propulsion Laboratory, California Institute of Technology, USA

ABSTRACT

With the discovery of extraterrestrial ocean environment, it is critical to develop unmanned vehicles with sensor payloads to explore the uncharted territory. The sensed data can be used to map the environment and seek signs of life. We present a design for a multi-modal sensing module consisting of 5 types of MEMS sensors integrated on a micro-swimming robot for extraterrestrial oceanographic exploration. The sensor module collects pressure, conductivity, temperature, pH, and biochemical data as the carrying robot traverses through the water body. In this paper, we discuss the design of the mentioned sensors on an AlGaN/GaN/Si wafer, as well as the fabrication and characterization of the conductivity, temperature, and pH sensors.

KEYWORDS

MEMS Sensor, Multi-Modal Sensing, Extraterrestrial Oceanographic Exploration.

INTRODUCTION

In this paper, we present a novel multi-modal sensing module for extraterrestrial oceanographic applications. The complete design has five sensing modalities to measure conductivity, temperature, pressure, pH, and biomarkers in unknown extraterrestrial water bodies. While individual sensors have been explored in various fields [1-4], our module provides a unified solution, allowing different sensors to coexist for compensation and correction during post-processing. The compact form-factor of a single MEMS chip replaces current discrete and bulky devices [5], making it ideal for integration in miniaturized vehicles.

This work is part of NASA JPL's Sensing with Independent Micro-swimmers (SWIM) project [6]. Recent discoveries have indicated the existence of liquid water under the icy crusts of moons in our solar system, such as Enceladus and Europa, namely, Ocean Worlds. Understanding the characteristics of these extraterrestrial oceans is crucial for scientific advancements. Table 1 summarizes the estimated properties of environment.

SWIM aims to deploy a swarm of micro-swimming robots in these water bodies to collect firsthand data about the uncharted territories (Figure 1). Each robot is equipped with the proposed sensing payload (Figure 2). Using swarm algorithms, robots are distributed across the domain and collectively map the environment spatially and temporally. The data is relayed back to a central mothercraft, i.e., Cryobot, which can enable implementation of advanced swarm behaviors such as source tracking for deeper understanding of the Ocean Worlds.

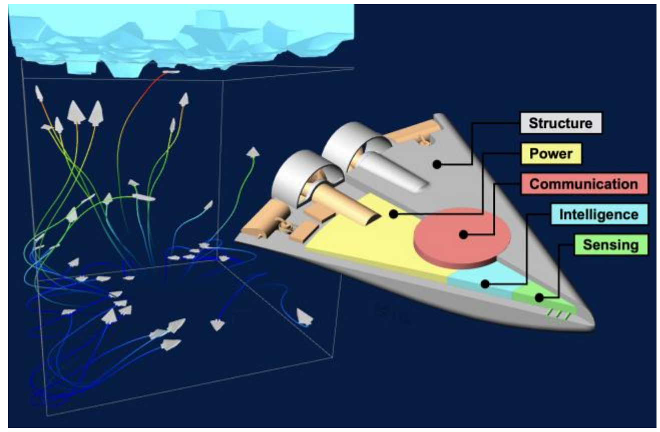

Figure 1: Operation concept of SWIM where micro-swimming robot swarm carries sensor payload.

Table 1: Estimates of Europa Ocean World environment properties.

Depth	20 – 40 km
Temperature	~273 K
Pressure	25 – 50 MPa (ice interface) 170 MPa (seafloor)
Conductivity	< 100 S/m

SENSOR DESIGN

Our 5-sensor MEMS module design is shown in Figure 2. The complete integration of all five sensors is currently underway. All sensors will be fabricated on a single AlGaN/GaN/Si wafer, with proper passivation with silicon nitride making it suitable for underwater environment. The final module will have design variations for each sensor to offer a selection of different dynamic ranges and sensitivities. The SEM images of the temperature, conductivity, pH, and pressure sensors are shown in Figure 3. The sensor designs are as follows:

- The **temperature** sensor consists of a platinum-based resistance temperature detector (RTD). The RTD are designed to have a nominal resistance ~15 kΩ at room temperature.

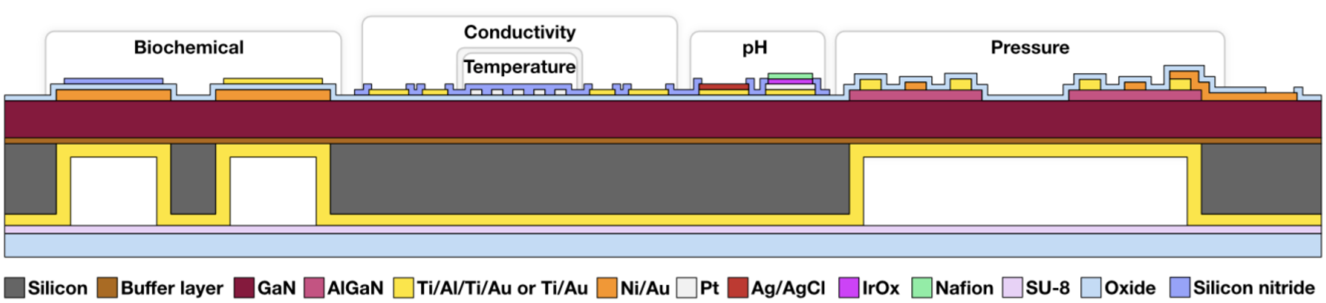

Figure 2: Cross-sectional schematic of the proposed multi-modal MEMS sensing module for SWIM.

978-1-940470-05-4/HH2024/$25©2024TRF
DOI 10.31438/TRF.HH2024.15

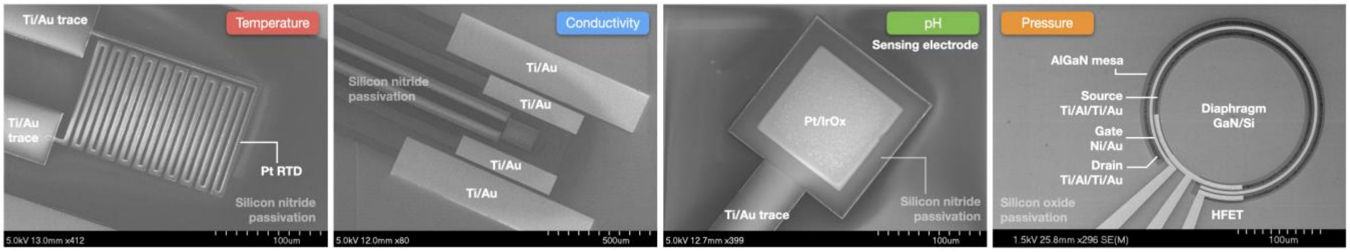

Figure 3: SEM images of the fabricated temperature, conductivity, pH, and pressure sensors.

- The **conductivity** sensor has 4 Ti/Au electrodes, where four-terminal measurement will collect water channel impedance. Current is applied to the outer pairs and voltage is measured across the inner pairs for impedance calculation.
- **pH** sensor consists of a sensing electrode, and a pseudo-reference electrode. The sensing electrode consists of a pH-sensitive iridium oxide (IrOx) layer, electrochemically deposited on a Pt layer following the recipe in [7]. The IrOx layer is encapsulated with Nafion, which is selectively permeative to hydrogen ion. A pseudo-reference electrode made of Ag/AgCl will provide reference potential. The open circuit potential (OCP) between the sensing and reference electrodes is indicative of the pH value.
- The **pressure** sensor consists of an AlGaN/GaN HFET fabricated on a circular diaphragm. In the linear region, the I-V characteristics of the HFET vary under the pressure-induced stress and can be modulated by the gate voltage [8].
- The **biochemical** sensor is a GaN resonator with top and bottom electrodes for actuation and different active layers deposited on top (nitride, oxide, and gold). As molecular species are immobilized on the top of the resonator, the mass change induces shift in resonance frequency. Due to different adsorption rates of biochemical materials such as proteins. Differential sensing among sensors is performed to differentiate the molecular species and their concentrations.

RESULTS

Here, we report on the characterization of three of the five sensors: temperature, conductivity, and pH sensors.

Temperature Sensor

The RTD temperature sensor is characterized over the range of interest from -0.5 to 45 °C. Resistance of the sensor shows linear dependency on temperature (Figure 4) with a sensitivity of 35.9 Ω/°C and a temperature coefficient of 0.00244 /°C at 20 °C.

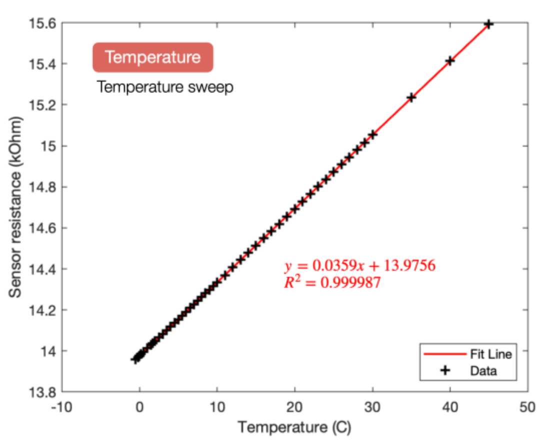

Figure 4: Temperature sensor resistance vs. temperature.

Figure 5 plots the transient response when the temperature is alternated between 15 °C and 45 °C, showing an average time constant of 6.75 seconds. The large time constant is attributed to the additional thermal mass of the packaging as the sensor is mounted on a PCB.

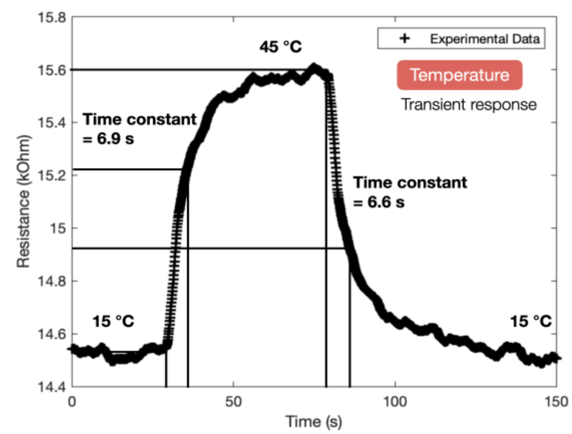

Figure 5: Measured transient response of the temperature sensor.

Conductivity Sensor

Figure 6 shows the resistance and conductance of the water channel as measured by the conductivity sensor. In the tested salinity range from 7.5 to 37.5 g/L NaCl, linear dependency of conductance versus salinity with a sensitivity of 7.24 μS/(g/L) is observed as expected.

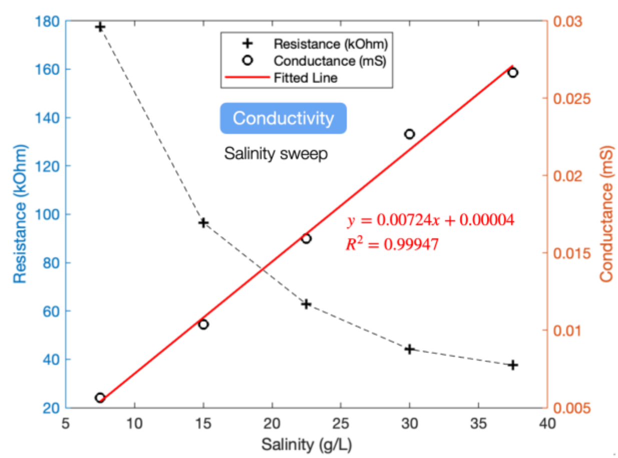

Figure 6: Conductivity sensor resistance and conductance vs. salinity.

Under constant salinity of 22.5 g/L, the conductivity sensor exhibits a temperature coefficient of -2.24 kΩ/°C (or 0.15247 /°C at

20 °C) as shown in Figure 7. This large temperature dependency suggests the necessity of having accompanying temperature sensor to correct conductivity reading for accurate salinity measurement. As designed, the temperature sensor is placed in the middle of the conductivity sensor channel to provide the most accurate local reading for temperature compensation.

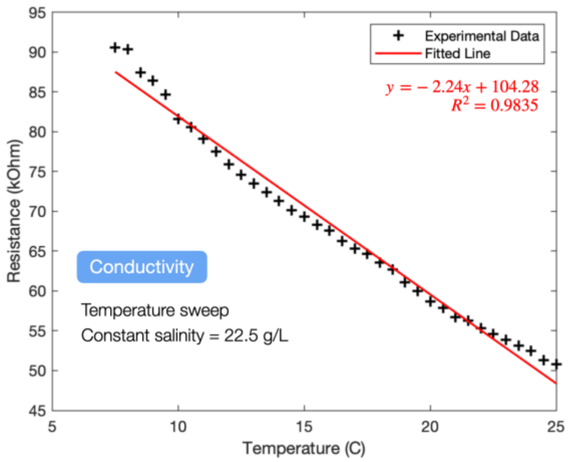

Figure 7: Temperature dependency of conductivity sensor resistance.

To test the stability of conductivity sensor as exposed to salty wafer for long operations, the sensor is stored in 37.5 g/L NaCl solution and the resistance across the salinity range is remeasured on day 8 and day 16. The result is plotted in Figure 8. Minimal change in resistance of 5.33% on average is observed with no visible deterioration of the gold electrodes under microscope, indicating that the sensor is suitable for long operations.

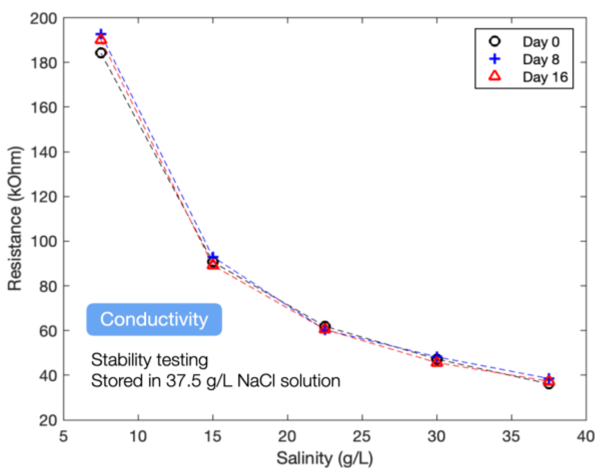

Figure 8: Stability of conductivity sensor stored in NaCl solution with salinity of 37.5 g/L.

pH Sensor

The pH sensor's open circuit potential (OCP) relative to a commercial glass Ag/AgCl reference electrode is plotted in Figure 9. Good linearity with a $R^2 = 0.9959$ is observed over the range of pH 4 to 10, with a sensitivity of -68.79 mV/pH. The sensitivity is consistent with literature for electrochemically deposited IrOx. Nonlinearity at pH of 11 is observed with a reduced sensitivity. The OCP stabilizes in less than 1 min after the sensor enters the environment, with a standard deviation after stabilization in each pH solution less than 0.5 mV. The pH of the testing sequence is as follow: 7→11→4→7. During the test, hysteresis (Figure 9) comparable to literatures [1, 7, 9] is observed with a maximum change in OCP of 22.46 mV at pH of 7.

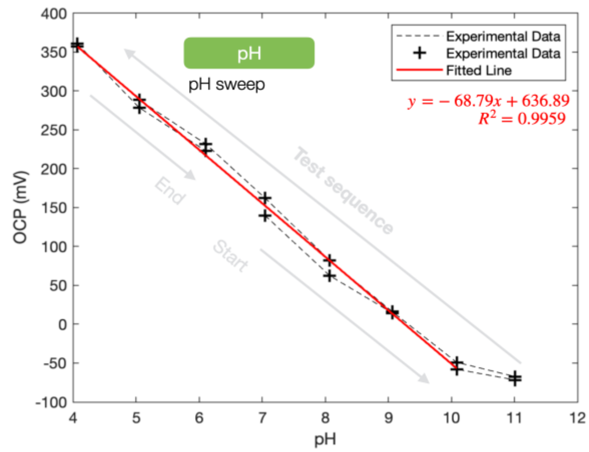

Figure 9: pH sensor OCP in a pH range of 4-11.

The temperature dependency of the pH sensor is a collective result from the temperature dependencies of both the sensing and reference electrode, as modeled by the Nernst equations:

$$E_{sen} = E_{sen}^{0} - 2.303\frac{RT}{nF}pH, \quad (1)$$

$$E_{ref} = E_{ref}^{0} - \frac{RT}{F}ln([Cl^{-}]), \quad (2)$$

where E_{sen} and E_{ref} are the half-cell potentials of the sensing and the reference electrodes, respectively, E_{sen}^{0} and E_{ref}^{0} are the standard half-cell potentials, R is the universal gas constant, T is the temperature, F is the Faraday constant, n is the number of electrons transferred in the IrOx reaction, and $[Cl^{-}]$ is the concentration of chlorine ion inside the glass reference electrode. The temperature dependency of OCP as the difference of E_{sen} and E_{ref} is plotted in Figure 10. As shown, the temperature coefficient is 0.69 mV/°C, which is 0.01 pH/°C for our sensor.

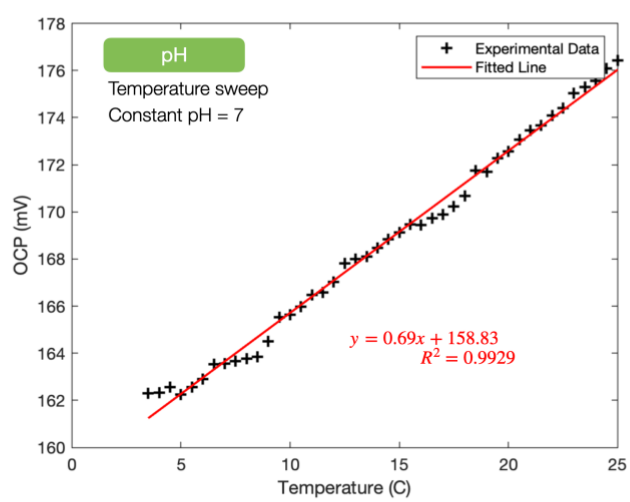

Figure 10: pH sensor temperature dependency.

The stability of pH sensor over long period of operation is tested under pH of 6, 7, and 8. The sensor is kept in each constant pH buffer solution for a testing duration of 5 hours. As shown in Figure 11, the average drift of OCP of the pH sensor is less than 0.52 mV/hour, with a standard deviation of 0.92 mV.

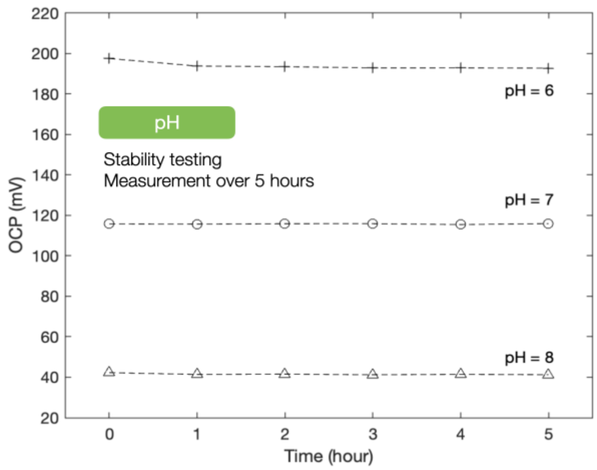

Figure 11: Stability of pH sensor in adjusted Tris buffer solution with pH of 6, 7, and 8.

Cations are known to interfere IrOx-based pH sensor, because they can participate in the ion exchange process in place of the hydrogen ion. The pH sensor is stored in 30.0 g/L NaCl solution for the duration of 13 days (Figure 12). An average drift of -6.08 mV/day is observed at pH = 7. The linearity across the pH range also deteriorates over the course of 13 days. However, the sensitivity (the slope) of the sensor remains stable of -67.49 ± 2.69 mV/pH. Thus, it is important to store and perform recalibration the sensor in stabilizing buffer solutions before deployment.

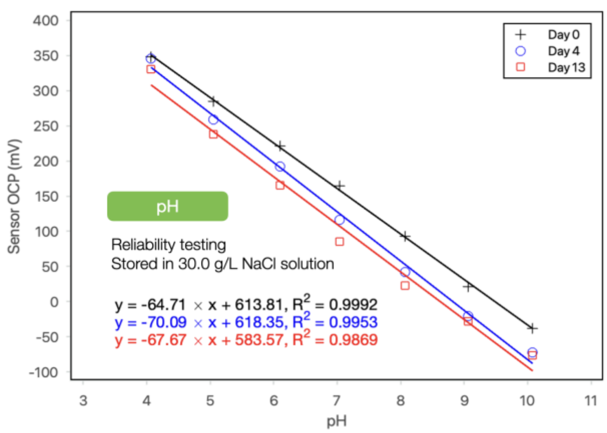

Figure 12: Reliability of pH sensor stored in NaCl solution with salinity of 30.0 g/L.

CONCLUSION

In this paper, we present the design of a comprehensive MEMS sensing module with a compact form-factor, suitable for the proposed micro-robotic swarm application in extraterrestrial oceanographic exploration. 5 sensors are integrated on a single AlGaN/GaN/Si substrate: HFET pressure sensor, GaN resonator biochemical sensor array, RTD temperature sensor, 4-port conductivity sensor, and IrOx pH sensor.

Preliminary results from the temperature, conductivity, and pH sensors showed good linearity, sensitivity, and stability. The cross-sensitivities among sensors, including the characterized temperature dependencies and the interference of cations on pH sensor, further demonstrates the advantage of multi-modal sensing. Future works on sensor data fusion to compensate these non-idealities will further improve the accuracies of all sensors.

With the development of the pressure and biochemical sensors underway and the on-going effort to integrate the MEMS module with micro-swimming robots, this work lays the foundation for advanced sensing required for scientific discoveries in these unexplored water bodies in the outer space.

ACKNOWLEDGEMENTS

The authors thank the NASA Innovative Advanced Concepts (NIAC) program for funding this project. The research was carried out in part at the Jet Propulsion Laboratory, California Institute of Technology, under a contract with the National Aeronautics and Space Administration (80NM0018D0004). U.S. Government sponsorship is acknowledged. The authors would like to thank the Institute for Electronics and Nanotechnology (IEN) at Georgia Institute of Technology for providing cleanroom facility, and Dr. Liu Nian, Alexandros Filippas, Dr. Farrokh Ayazi, Dr. Zhenming Liu, Dr. Durga Rao Gajula, Ting-Ying Yu, and Isha Lodhi for the help and advice during the development.

REFERENCES

[1] L. Manjakkal, S. Dervin, and R. Dahiya, “Flexible potentiometric pH sensors for wearable systems”, *RSC advances*, 10, 15 (2020), pp. 8594-8617.

[2] D. He, M.A. Shannon, and N.R. Miller, “Micromachined Silicon electrolytic conductivity probes with integrated temperature sensor”, *IEEE Sensors Journal*, 5, 6 (2005), pp. 1185–1196.

[3] D. Gajula, I. Jahangir, and G. Koley, “High temperature AlGaN/GAN membrane based pressure sensors”, *Micromachines*, 9, 5 (2018), pp. 207.

[4] K. Brueckner, F. Niebelschuetz, K. Tonisch, C. Foerster, V. Cimalla, R. Stephan, J. Pezoldt, T. Stauden, O. Ambacher, and M.A. Hein, “Micro-and nano-electromechanical resonators based on SiC and group III-nitrides for sensor applications”, *physica status solidi (a)*, 208, 2 (2011), pp. 357-376.

[5] C. Albaladejo, P. Sánchez, A. Iborra, F. Soto, J.A. López, and R. Torres, “Wireless sensor networks for oceanographic monitoring: A systematic review”, *Sensors*, 10.7 (2010), pp. 6948-6968.

[6] E.W. Schaler, A. Ansari, S.M. Howell, H.J. Lee, M.W. Smith, A. Rajguru, L.P. Tosi, Z. Hao, and J.D. Kim, “SWIM-Sensing with Independent Micro-swimmers”, *The Astrobiology Science Conference (AbSciCon) 2022* (2022), pp. 417-05.

[7] S.A.M. Marzouk, “Improved electrodeposited iridium oxide ph sensor fabricated on etched titanium substrates”, *Analytical Chemistry*, 75, 6 (2003), pp. 1258–1266.

[8] U.K. Mishra, P. Parikh, and Y.F. Wu, “AlGaN/GaN HEMTs - an overview of device operation and applications”, *Proceedings of the IEEE*, 90, 6 (2002), pp. 1022-1031.

[9] H.J. Chung, M.S. Sulkin, J.S. Kim, C. Goudeseune, H.Y. Chao, J.W. Song, S.Y. Yang, Y.Y. Hsu, R. Ghaffari, I.R. Efimov, and J.A. Rogers, “Stretchable, multiplexed pH sensors with demonstrations on rabbit and human hearts undergoing ischemia”, *Advanced healthcare material*, 3, 1 (2014).

CONTACT

*A. Ansari, email: azadeh.ansari@ece.gatech.edu